

Development and Evaluation of an Advanced Aluminum Alloy for Additive Manufacturing

Rebecca A Sweny^{1*}, Jay F Tressler² and Richard P Martukanitz^{1,2}

¹Department of Materials Science and Engineering, Pennsylvania State University, University Park, PA 16801, USA

²Center for Innovative Materials Processing through Direct Digital Deposition, Pennsylvania State University, University Park, PA 16801, USA

Abstract

Experiments were conducted on several alloys representing the Al-Cu-Ag-Mg system to determine the applicability of using these alloys for AM. Alloys were formulated and prepared utilizing a powder blending technique using a pre-alloyed master alloy powder containing Al, Mg, Ti, and Zr with elemental powders of pure Cu and Ag. These powder were processed using laser-based directed energy deposition to produce specimens that were treated to represent the post-process aged only and post-process solution heat treated and aged conditions. Microhardness and microstructural characterization was then conducted. Results of this investigation showed that an aluminum alloy containing between 6 and 8% Cu and 1 to 4% Ag, while also containing 0.3% Mg, Ti, and Zr, displayed excellent response to precipitation strengthening for both post-process treatments. Alloys that were completely solutionized and aged after processing were able to achieve microhardness values exceeding 180 VHN, which are significantly higher than the commonly used Al-10Si-0.5Mg alloy for AM processes. The high microhardness achieved with the experimental alloy could be attributed to a uniformly distributed network of fine θ' and Ω precipitates, which was confirmed through TEM. Depending upon the desired post processing treatment (aging only or solutionizing and aging), the results indicate that an alloy composition within this system may be defined to provide optimal strength.

Keywords: Materials for additive manufacturing; Aluminum alloy; Aluminum for additive manufacturing; Advanced aluminum alloy; Metals additive manufacturing; Metals; Aluminum

Introduction

Throughout industry, aluminum alloys have been used in applications requiring light weight, moderate strength, and good general corrosion resistance. Many of these alloys are based on the precipitation strengthened (heat treatable) aluminum alloy systems that provide ultimate strengths between 310 MPa, for alloy 6061-T6, and 570 MPa, for alloy 7075-T651 [1]. However, in applications where the design is dominated by specific strength, high strength alloys, such as 2219-T851, 2024-T851, and 7075-T651, are broadly employed. All of these alloys are readily available in sheet and plate product form and possess good formability and machinability, enabling them to be fabricated into complex parts and used in a wide range of applications. However, the use of additive manufacturing (AM) for producing aluminum components has been limited to the Al-10Si-0.5Mg alloy, which is based on a casting alloy composition having low sensitivity to solidification cracking and moderate strength [2]. Although this alloy is being utilized extensively for AM, the properties of the alloy hinder its use in applications requiring higher strength. If an aluminum alloy that approaches the strength of current high strength aluminum alloys, while also being suitable for AM, becomes available, significant opportunities will arise within various industry sectors. This alloy would fully exploit the benefits of AM in a broad range of applications requiring high strength and low weight. A comparison of typical ultimate tensile strength of several precipitation strengthened aluminum alloys, along with the Al-10Si-0.5Mg alloy is shown in Figure 1 [1,3]. In Figure 1, typical strength is shown for material represented by the various alloy and temper designations, except for the Al-10Si-0.5Mg alloy, which represents a post-process stress relief at 300°C for 2 hours. As illustrated in the figure, there may be significant opportunities to expand the application of AM of aluminum if an alloy could be identified to approach the properties of high strength aluminum alloys that are currently available. Hence, the focus of this research was to develop an aluminum alloy having significantly

improved strength over the Al-10Si-0.5Mg alloy, while also offering characteristics and attributes required for the AM process.

Alloy Design Approach

The alloy design criteria that was employed during development

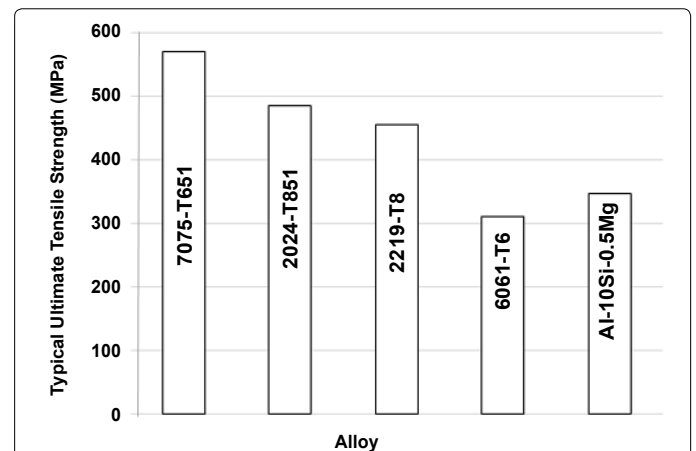


Figure 1: Typical ultimate tensile strength of several high strength aluminum alloys in comparison to the Al-10Si-0.5Mg alloy currently used for additive manufacturing (alloy Al-10Si-0.5Mg represents post-process stress relief at 300°C for 2 hours) [1,3].

***Corresponding author:** Rebecca A Sweny, Materials Science and Engineering Department, Pennsylvania State University, University Park, PA 16801, USA, Tel: 8146024254; E-mail: rsweny33@gmail.com

Received December 10, 2018; **Accepted** December 20, 2018; **Published** December 30, 2018

Citation: Sweny RA, Tressler JF, Martukanitz RP (2018) Development and Evaluation of an Advanced Aluminum Alloy for Additive Manufacturing. J Material Sci Eng 7: 505. doi: [10.4172/2169-0022.1000505](https://doi.org/10.4172/2169-0022.1000505)

Copyright: © 2018 Sweny RA, et al. This is an open-access article distributed under the terms of the Creative Commons Attribution License, which permits unrestricted use, distribution, and reproduction in any medium, provided the original author and source are credited.

entailed maximizing strength while ensuring the ability of the alloy to be processed using AM. To achieve these qualities, a unique precipitation hardenable alloy system was identified that exhibited nil sensitivity to solidification cracking and would be considered chemically stable in powder form prior to and during AM processing. This resulted in an alloy being identified based on the Al-Cu-Ag-Mg system [4]. These alloys exhibit a significant response to precipitation strengthening, show very low sensitivity to solidification cracking, preserve the quality of powder prior to processing, minimize vaporization losses of important alloying elements during processing, provide a stable oxide that has a relatively low hygroscopic nature, and show improved surface quality during the AM process [4-9].

The most widely used aluminum alloy for AM is designed around the Al-Si system; however, as alluded to earlier, most alloys used in engineering applications are based on alloying elements such as Cu, Mg, Zn, and Si to produce precipitation strengthening phases. To be used in additive manufacturing, these alloys must have inherent characteristics that enables them to be processed by AM. An important consideration is good weldability, which is primarily identified as sufficient resistance to solidification cracking. The susceptibility to solidification cracking for alloys of aluminum have been well established through experimentally derived solidification-cracking curves, which have been empirically developed to assess solidification cracking based on composition. These curves represent solidification cracking sensitivity based on a composition reflecting a binary, ternary, or quaternary alloying system. Shown in Figure 2 is solidification crack sensitivity exhibited by the Al-Cu-Mg alloy system under solidification rates and thermal stresses dictated by welding [7]. In the figure, crack sensitivity is shown as contour lines for total crack length based on the amount of copper and magnesium within the alloy for the aluminum-rich corner of compositions. Alloys containing relatively high levels of Cu and low levels of Mg, owing to a decrease in the amount of the Al-Cu-Mg ternary eutectic [10], are relatively insensitive to solidification cracking, and hence, are of interest in the present study.

High levels of Cu in Al-Cu alloys have historically been used for welding applications requiring low solidification crack sensitivity, and they have also been used for AM. Research by Taminger and Hafley have shown microstructures of alloy 2219, having a nominal Cu content of 6.3% and produced using the electron beam-based directed energy deposition process, to be free of cracking and exhibit complete layer fusion with very little porosity [5-8]. In Al-Cu alloys containing moderate amounts of Mg, such as 2519, additions of Cu above 6% and

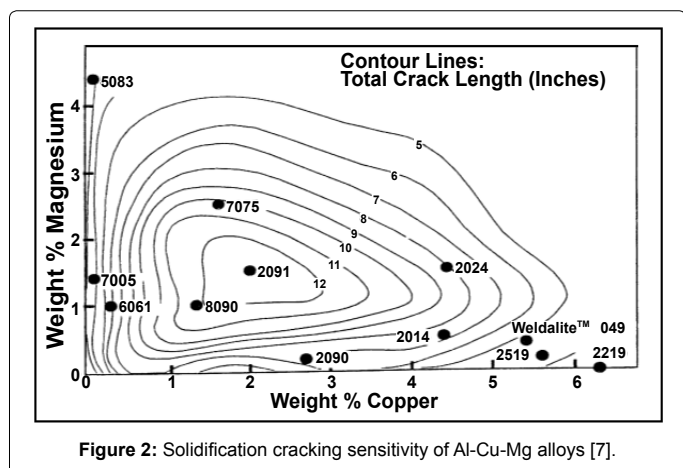


Figure 2: Solidification cracking sensitivity of Al-Cu-Mg alloys [7].

controlling Cu content to below 0.5% have been found to exhibit very low sensitivity to solidification cracking during welding [11].

Another important alloy design consideration is strength, which for the alloy system being considered involves optimizing the precipitate strengthening reactions. In the Al-Cu-Mg system, the precipitates that may exist include θ (Al_2Cu), S (Al_2CuMg), and T (Al_6CuMg_4) [12-14]. Figure 3 shows the aluminum rich corner of the Al-Cu-Mg phase diagram, indicating the precipitate phases that form as a function of composition after long term aging at 190°C [7]. When added to Al-Cu-Mg, Ag has shown to stimulate an increased age hardening reaction [15,16]. Teleshov et al. stated that the effect of Ag on precipitation in Al-Cu-Mg is connected with the changes in the solid solution mechanism of decomposition during artificial aging [17]. Hence, the addition of Ag promotes the formation of each precipitate. In the Al-Cu-Mg alloy, the primary strengthening precipitate relies on the Cu/Mg ratio [15,18,19]. For an advanced aluminum alloy for engineering components, the area of interest lies in the $\alpha+\theta$ region of Figure 3, where the alloy possesses a very high Cu:Mg ratio.

The θ (Al_2Cu) phase is an equilibrium precipitate that forms in materials with a high Cu:Mg ratio [20]. θ possesses a body centered tetragonal structure on the {100} planes in the aluminum matrix, but with the addition of Ag, Al_2Cu takes on a different form, designated Ω . The Ω (Al_2Cu) phase precipitates as thin hexagonal plates which grow on the {111} planes in the aluminum matrix [21,22]. In this high Cu:Mg region, with the addition of Ag, Ω precipitates form a fine, uniform strengthening network. The precipitation sequence in an Al-Cu-Ag-Mg alloy with a high Cu:Mg ratio is as follows [14,23-26]:

$\alpha_{\text{SSS}} \rightarrow \text{Mg-Ag co-clusters} \rightarrow \Omega \text{ phase} + \theta' \text{ phase} \rightarrow \theta + \text{Mg, Ag, Cu enriched phases}$.

During precipitate formation, Ag traps Mg atoms creating clusters which then act as heterogeneous nucleation sites for Ω [27]. The Ω precipitation is achieved by the diffusion of Cu atoms to these Mg-Ag clusters where they grow into platelets until the concentration of Cu reaches that of Ω (Al_2Cu) [19]. Although the chemistry and crystal structure of Ω is very similar to that of equilibrium θ , these precipitates are a variation of θ that result from the collaboration between Mg and Ag [9]. θ' precipitates form concurrently with Ω during aging [14]. Xiao et al. and Bai et al. found that increasing the amount of Ag and Cu lead

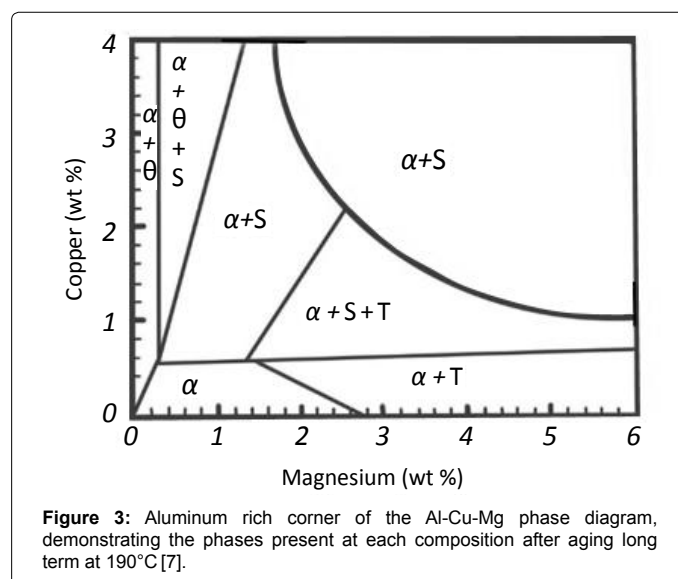


Figure 3: Aluminum rich corner of the Al-Cu-Mg phase diagram, demonstrating the phases present at each composition after aging long term at 190°C [7].

to more growth of the Ω phase, resulting in improvements in strength [21,27]. Because Ω are coherent precipitates, they are able to withstand shearing by dislocation, making them a very efficient strengthening agent if uniformly distributed to form a network of precipitates [25]. This is achievable through peak aging. The Ω precipitates are found to occur on aging above 100°C and are stable and coherent up to an aging temperature of about 250°C [20,25,28].

The Al-Cu-Ag-Mg alloys have shown promising material properties for use in advanced applications because of their high strength to density ratio, good heat resistance, good durability and corrosion resistance, good machinability and formability, low cost, and ready availability [21,23,29]. Prior work on this system by Al-Obaisi et al. has found that while Ag is required to precipitate Ω , additions of Ag to Al-Cu without Mg does not precipitate Ω [9]. The cooperation of Mg and Ag is essential to the formation of the Ω precipitate [30]. Huang et al. found that the Al-Cu-Ag-Mg system showed increased mechanical properties over Al-Cu-Mg with no Ag or Al-Cu-Ag with no Mg [31]. The Al-Cu-Ag-Mg alloys strengthened by the dispersion of Ω phase precipitates have also been found to provide a combination of high strength, good fracture toughness, and improved creep resistance over Al-Cu-Mg alloys [14]. Previously researched wrought alloys based on this system have shown tensile strengths of 459 MPa, 499 MPa, and 534 MPa, to be achievable [20,21,23]. The potential of these new alloys are being explored for applications within the aerospace industry, with several programs already researching Al-Cu-Mg-Ag wrought alloys for use in the new-generation of supersonic passenger aircraft [17].

Other considerations for an advanced aluminum alloy for AM regards the impact of the alloy on the process. The AM process, as it pertains to metallic systems, utilizes a high intensity laser or electron beam to melt and resolidify material at relatively high solidification and cooling rates. Deposition of the numerous layers that forms the three dimensional object also results in significant residual stress being generated during the process. In many instances, the feedstock used to produce the object is in powder form and the characteristics of the powder, especially at the surface, may play an important role in consistency of the process and quality of the material produced.

Based on the desire to create an alloy having improved strength, as well as the considerations above, an advanced aluminum alloy system was formulated. Compositions of interest were broadly based on the Al-Cu-Ag-Mg system, with alloying levels being established to maximize strength and optimize processing within AM systems. As described above Cu, Ag, and Mg play a role in establishing the precipitation network responsible for developing strength. Higher levels of Cu, coupled with controlled levels of Mg, would minimize sensitivity to solidification cracking. The majority of the primary alloying elements involve species, notably Cu and Ag, having higher vapor pressure than aluminum in the liquid form and act to minimize vaporization losses that are prevalent under high energy intensity processing. Although Mg is an active alloying element, its content would be kept low to reduced crack sensitivity, minimize vaporization, and suppress the formation of thick Mg-oxide (MgO) on the surface. Small amounts of Mg in aluminum have been found to reduce oxidation, with higher content resulting in the formation of MgO films that readily hydrate in the presence of low levels of moisture to Mg(OH)₂ [32]. The chemical absorption of moisture to form a hydrated surface on aluminum powder during storage or processing can have significant impact on the reliability of the process and potential for forming hydrogen porosity within the builds [33,34]. Surface tension driven forces within the melt pool may also alter the deposition geometry during processing,

which may be operative during the build process due to residual heat or varying parameters, and may be influenced by local composition. Additions of Cu and Ag do not influence surface tension of liquid aluminum, and small amounts of Mg have a negligible effect [1]. Finally, the use of small additions of Ti and Zr have been historically used for grain refinement in aluminum alloys, and this would also be reflected in an advanced aluminum alloy for AM.

Experimental

Considering the requirements for an advanced aluminum alloy for AM, several alloys of interest representing the Al-Cu-Ag-Mg system were blended using powers, which were subsequently used to produce material through the directed energy deposition (DED) AM process for evaluation. The range of alloying additions to aluminum that were selected for evaluation comprised 6, 7, and 8 percent Cu and 2, 3, and 4 percent Ag. The target level of Mg was held constant at approximately 0.3 percent, and small additions of Ti and Zr (0.3%) were also included in all alloys. A full factorial design was used to develop an experimental plan which consisted of 2 variables (Cu and Ag) at 3 compositional levels, yielding 9 total compositions. These 9 target compositions were produced by blending a pre-alloyed Al-0.35Mg-0.30Ti-0.30Zr master alloy powder with additions of pure Ag powder and pure Cu powder to achieve the desired alloy compositions. Table 1 represents the 9 targeted alloy compositions.

The master alloy was argon atomized by Kymera International/Ecka Granules, and was blended with a 99.9% pure Cu powder and 99.98% pure Ag powder to obtain the desired target compositions. The elemental Cu and Ag powder were inert gas atomized by American Elements. A powder sieve size of -150/+325 ($d_{10}=50 \mu\text{m}$, $d_{50}=75 \mu\text{m}$, $d_{90}=100 \mu\text{m}$) was used for all powders to encourage blending and accommodate the powder requirements for the DED process. The size distribution of the powder used for blending was confirmed using a Malvern Mastersizer 2000. Target compositions were blended based on weight additions of Cu and Ag powder to 800 g of the master alloy powder for each composition and blended using a rotary-style mixer for 60 minutes. Three blended powders representing three target compositions were also chosen at random and characterized using the Malvern Mastersizer 2000 to verify the powder size range of the blends.

Deposits representing the experimentally blended powders were produced using the High Power High Deposition (HPHD) system at the Center for Innovative Materials Processing through Direct Digital Deposition (CIMP-3D) at the Pennsylvania State University. Experiments were conducted using a 12 kW ytterbium laser, custom deposition head, and processing chamber for inert gas. The processing head utilized water-cooled reflective optics having a 600 mm focal length from a parabolic focus mirror. Powder was provided using four nozzles positioned at the 90° quadrants with each nozzle being position

Alloy	Cu (wt %)	Ag (wt %)	Mg (wt %)	Ti (wt %)	Zr (wt %)
1	6	2	0.3	0.28	0.2
2	6	3	0.3	0.28	0.2
3	6	4	0.3	0.28	0.2
4	7	2	0.3	0.28	0.2
5	7	3	0.3	0.28	0.2
6	7	4	0.3	0.28	0.2
7	8	2	0.3	0.28	0.2
8	8	3	0.3	0.28	0.2
9	8	4	0.3	0.28	0.2

Table 1: Characteristic alloy compositions achieved by blending to be additively manufactured.

30° off the beam axis. The nozzles, having an inside diameter of 2 mm, were positioned 10 mm off of the substrate. Processing was conducted below the focal length at a position that provided a laser spot size of 3.5 mm in diameter.

Deposits representing each powder blend was produced using approximately 6 tracks in the horizontal plane and multiple layers to achieve a build height of 100 cm using a hatch or track spacing of 2.5 mm. Build height per layer was approximately 0.8 mm using a powder flow rate of 7.8 g/min. Laser power was 3.0 kW to the part at a travel velocity of 10.6 mm/s. The build chamber utilized an argon atmosphere having an oxygen level of approximately 100 ppm, and argon gas was provided to assist powder feeding at a rate of 3.0 l/min. Employing these parameters, the powder blends were used to deposit material onto a 12.7 mm thick aluminum alloy 6061 substrate to produce specimens approximately 20 mm wide, 200 mm in length, and 100 mm in height. Alloys 1 through 7 were successfully printed on 6061 aluminum plates to produce material for testing. Powder representing Alloys 8 and 9 were compromised due to extremely humid storage conditions and therefor were not processed.

After producing the specimens, a sample of each alloy was obtained from the center portion of each build at a height of approximately 50 to 60 mm from the substrate. These samples were forwarded to Westmoreland Mechanical Testing & Research Inc. for chemical analysis by inductively coupled plasma (ICP). Samples were tested for Cu, Ag, Mg, Zr, and Ti content. These measured compositions for each alloy, excluding Alloys 8 and 9, are displayed in Table 2.

A set of two slices from each build were obtained for evaluating properties and characteristics of the material after post process heat treatments. These slices were also examined using optical microscopy for indication of deposition characteristics, porosity, and cracking. The two post process heat treatments evaluated were post-process aged only and post-process solution heat treated and aged conditions. These slices were obtained by removing the cross-sections from the center plane along the build length, and each slice was approximately 8 mm in thickness. These cross-sectional slices were further subdivided into 12 samples approximately 10 mm wide and 17 mm high; all being approximately 8 mm in thickness. These 12 samples were randomly selected for use in the two post process heat treatment experiments. Post-process aging only experiments were conducted using a Omegalux LMF-3550 box furnace at a temperature of 160°C for 0, 2, 4, 8, 12, 16, 20, 24, and 28 hours. Samples that were evaluated for post-process solution heat treatment and aging were solutionized using the same furnace at 510°C for 75 minutes, followed by a water quench and aging at 160°C for 0, 2, 4, 8, 12, 16, 20, 24, and 28 hours.

After the heat treating experiments, Vickers hardness measurements were taken on a LECO M-400-GI microhardness indenter. Averages of 10 microhardness measurements were obtained for each sample representing the 7 compositions for the post-process

aged only and post-process solution heat treated and aged conditions. Selected samples were also characterized by various techniques. Samples of Alloy 1, representing the peak aged condition after solution heat treatment and aging (solution treated and aged for 20 hours), were cold mounted and etched in Keller's reagent. These samples were then imaged using optical microscopy and scanning electron microscopy. An additional sample of Alloy 1 representing this condition was also utilized for transmission electron microscopy after thinning using a focused ion beam. Optical micrographs were obtained on a Nikon Epiphot inverted metallurgical microscope. Images from the SEM were taken on the Quanta 250 SEM, and TEM images were obtained using a FEI Talos F2000x microscope.

Results and Discussion

Optical microscopy conducted at low magnification (100X) indicated that small spherical porosity in limited amounts was present in all of the builds; however, no indication of solidification cracks was observed. The porosity that was present was believed to be due gas absorption of hydrogen [34], potentially present in the powder or from absorption of moisture on the surface of the powder particles. Although the processing chamber provided a controlled inert atmosphere, high humidity was present in the area of the AM system, which could of enabled contamination of the powder prior to processing.

The results of Vickers microhardness testing is shown in Figures 4 and 5 for the post-process aged only and post-process solution heat treated and aged conditions, respectively. Microhardness measurements for all alloys, which is displayed using the measured compositions for Cu and Ag, show promising result for an advanced aluminum alloy, with every alloy exceeding the typical hardness of the Al-10Si-0.5Mg, reported to be 100 VHN [3] after solution heat treating and aging. All 7 alloys in the solution heat treated and aged condition achieve peak hardness between 150 VHN and 180 VHN. It must be noted that the experimental alloys were blended from elemental powder, which may have resulted in nonhomogeneous compositions throughout the build; however, based on the variability of the data, which is represented in the figures as error bars depicting ± one standard deviation, it is believed that the changes in alloying concentration representing the 10 mm by 17 mm samples were not substantial.

The curves representing post-process aging only at 160°C (Figure 4) indicated that some response to precipitation strengthening was operative during aging. Alloy 7 containing 7.7 Cu and 1.9 Ag exhibited the shortest time to achieve peak aging, with Alloys 2, 4 and 6 showing peak hardness at aging time between 16 and 20 hours. As mentioned earlier, although variability in composition could be expected, there appears to be a trend in time for peak aging based on the amount of Cu (Alloy 2 containing 4.9 Cu, Alloy 4 containing 5.4 Cu, and Alloy 6 containing 6.6 Cu). There appears to be a trend in the data for the peak microhardness obtained during prolong aging, with the level of Cu also

Alloy #	Target Compositions	Tested Compositions (wt %)				
		Cu	Ag	Mg	Zr	Ti
Alloy 1	Al-6Cu-2Ag-0.28Mg-0.28Ti-0.20Zr	4.91	1.39	0.20	0.20	0.29
Alloy 2	Al-6Cu-3Ag-0.28Mg-0.28Ti-0.20Zr	4.87	2.34	0.19	0.21	0.28
Alloy 3	Al-6Cu-4Ag-0.28Mg-0.28Ti-0.20Zr	4.44	2.64	0.21	0.21	0.28
Alloy 4	Al-7Cu-2Ag-0.28Mg-0.28Ti-0.20Zr	5.43	1.48	0.23	0.22	0.29
Alloy 5	Al-7Cu-3Ag-0.28Mg-0.28Ti-0.20Zr	5.46	2.19	0.19	0.21	0.28
Alloy 6	Al-7Cu-4Ag-0.28Mg-0.28Ti-0.20Zr	6.64	3.40	0.21	0.20	0.26
Alloy 7	Al-8Cu-2Ag-0.27Mg-0.26Ti-0.19Zr	7.74	1.87	0.21	0.22	0.29

Table 2: Chemical Analysis of each blended experimental alloy measured by inductively coupled plasma.

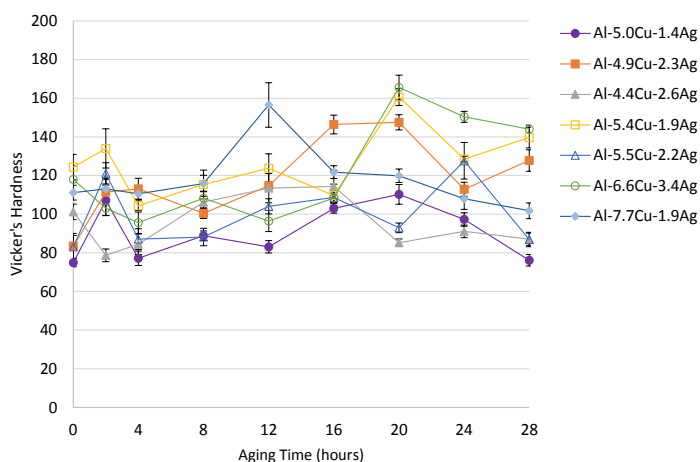


Figure 4: Average Vickers hardness measurements of post-process aged only samples, aged at 160°C.

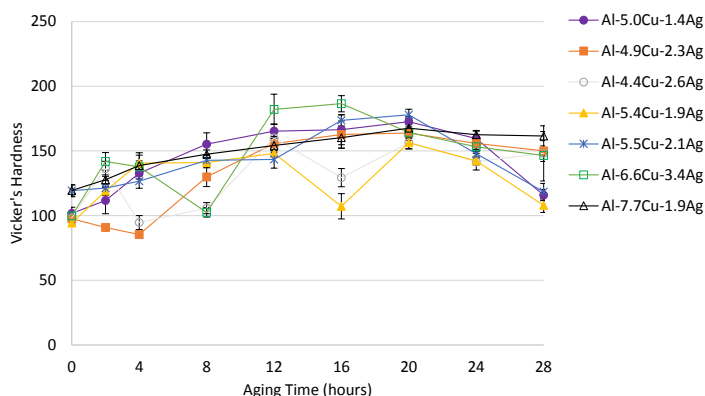


Figure 5: Average Vickers hardness measurements of samples solution heat treated at 510°C and aged at 160°C.

reflecting maximum hardness achieved. Several of the experimental alloys (Alloy 2, 4, 6, and 7) attained hardness values after peak aging that significant exceeded the hardness expected from the Al-10Si-0.5Mg alloy after stress relief.

The microhardness values for samples that were post-process solution heat treated at 510°C and aged at 160°C indicated results more akin to classical aging or precipitation strengthening. The curves for this treatment (Figure 5) reflect a full aging curve having characteristics of under, peak, and over aging. Alloy 6 containing 6.6% Cu and 3.4% Ag exhibited the fastest peak aging and the highest microhardness, which exceeded 180 VHN. Alloy 1 (5.0% Cu and 1.4% Ag) and Alloy 5 (5.5% Cu and 2.1% Ag) also displayed high peak hardness but at aging time approaching 20 hours. In one case, Alloy 2 having 4.9% Cu and 2.3% Ag, showed a decrease in microhardness during the initial stage of aging after solutionizing, which may be indicative of a reversion process in the alloys lean in Cu. Although the results indicated by the microhardness data after solution heat treatment and aging clearly show a response to precipitation strengthening, caution was observed in drawing definitive conclusions based on composition and response to aging because of potential inhomogeneity within the slices used to obtain the heat treatment samples.

The aging curves after solutionizing for Alloy 1 (Al-5.0Cu-1.4Ag) showed a consistent increase in hardness until reaching the peak age

condition at 20 hours. The peak hardness of the solution heat treated and aged sample was 173 VHN, while the peak hardness of the post-process aged only sample was 110 VHN. The aging curves for this alloy are displayed in Figure 6. Because of the high hardness after peak aging paired with the consistent aging observed for this alloy, it was chosen for further characterization in the solution heat treated and peak aged condition. Because of the high microhardness exhibited at peak aging after post-process aging only (166 VHN) and post-process solution heat treatment and aging (186 VHN), Alloy 6 (Al-6.6Cu-3.4Ag) was also further evaluated by mapping microhardness after solutionizing and peak aging with local composition for the entire build slice.

The combined aging curves for Alloy 6 is shown in Figure 7. The as-built aging curve for this alloy displayed a slight drop in hardness initially, with the peak age hardness of 165 VHN being reached after 20 hours. The post-process solution heat treated and aged curve showed a significant dip in hardness after 8 hours of aging, followed by a rapid increase to the peak age condition after 16 hours, with a peak hardness of 187 VHN. Alloy 6 achieved the highest peak age hardness value of all tested alloys. This alloy targeted a combination of high copper and high silver contents, encouraging high amounts of Ω precipitation.

A comparison of peak-age microhardness after solution treatment and aging for experimental Alloys 1 and 6 to hardness values of selected commercial aerospace and additive manufacturing alloys is illustrated

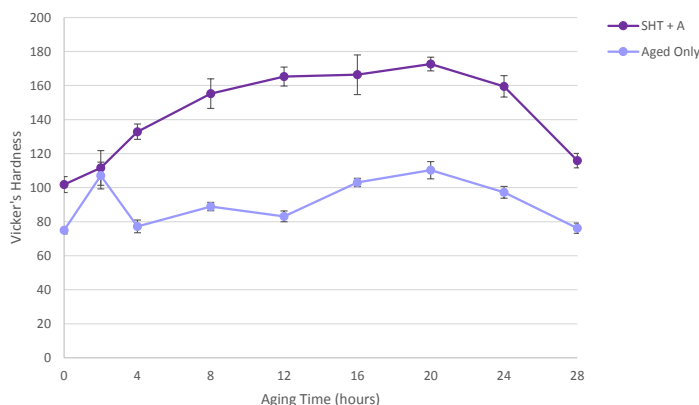


Figure 6: Aging curves for Alloy 1 after solution heat treatment at 510°C and aging at 160°C for 28 hours and after as-built aging at 160°C for 28 hours.

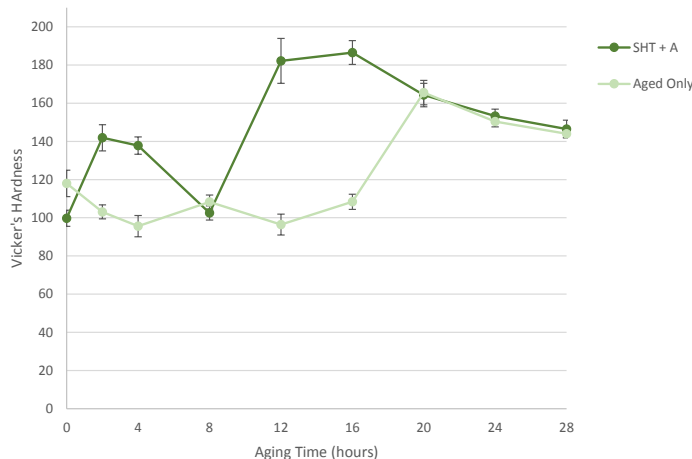


Figure 7: Aging curves for Alloy 1 after solution heat treatment at 510°C and aging at 160°C for 28 hours and after as-built aging at 160°C for 28 hours.

in Figure 8. Alloy 1 attained peak hardnesses averaging 173 VHN after solution heat treatment at 510°C and aging for 20 hours at 160°C, while Alloy 6 attained peak hardnesses averaging 186 VHN after solution heat treatment at 510°C and aging for 16 hours at 160°C. Alloy Al-10Si-0.5Mg is reported to attain a hardness of 100 VHN after being stress-relieved at 300°C for 2 hours, or 123 VHN if left in the as-built condition [35]. The literature indicates alloy 6013-T651 attains a peak hardness of 149 VHN [36], alloy 2024-T6 achieves a peak hardness of 142 VHN, and alloy 7075-T6 exhibits a peak hardness of 175 VHN [37,38]. Based on results of microhardness measurements, which is illustrated in Figure 8, it appears that the experimental alloy system shows significant promise in offering improved strength for AM applications.

As was mentioned, Alloy 1 was selected for additional microstructural characterization. Optical micrographs of this alloy, after post-process solution heat treatment and aging for 20 hours at 160°C to obtain the peak-age condition, are shown in Figures 9 and 10 for perspectives in both the x-direction and the z-direction of the build, respectively. Strengthening precipitates were not expected to be observed at these magnifications; however, black/dark purple and grey second phases were visible, as pointed out by red arrows on the micrographs. In the z-direction, grain boundaries were visible at high magnification (500X) and appeared to show a fine cellular structure. In order to identify these phases, samples were further characterized

using SEM. The images for Alloy 1 in the post-process solution heat treated and peak aged condition are shown in Figure 11. Along with the secondary electron image are EDS maps for Al, Cu, Ag, Ti, and Fe obtained for precipitates visible within the image. It was observed from the EDS maps, and anticipated, that the aluminum matrix contained evenly dispersed silver, copper, iron, and titanium with the bright white precipitates contain primarily aluminum, copper, and iron. It is believed that the large, white precipitates represent the equilibrium Al_2Cu phase or a ternary composition containing Al, Cu, and Fe.

Additionally, EDS point measurements were taken to better identify the composition of the matrix and intergranular constituents. Figure 12 displays a SEM image and elemental spectrums obtained through EDS of an area near the image obtained in Figure 11. The image includes several grain boundaries with one boundary exhibiting a long thin constituent or segregation at the grain boundary, which is identified as Spectrum 6 on the image. The elemental spectrums for this constituent indicated a semi-quantitative composition of 77% Al, 15% Cu, 2% Fe, and 1% Ag. Analysis of other grain boundary constituents also showed similar compositions but with variation in Cu and Fe. Oxygen was also identified in the spectrum, but was probably attributed to sample contamination. Based on the results of the SEM and EDS analysis, it is believed that the formation of eutectic compositions, potentially ternary or higher, resulted in segregation at grain boundaries during initial solidification and partially remained upon solutionizing. As

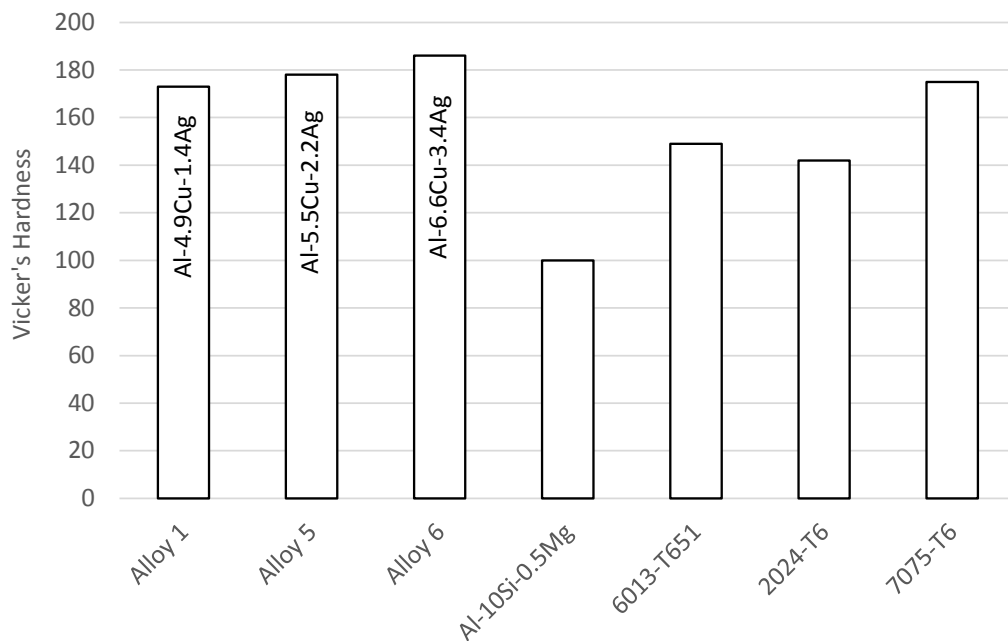


Figure 8: Comparison of hardness of experimental alloys with commercial alloys at peak-age condition [3,35-37].

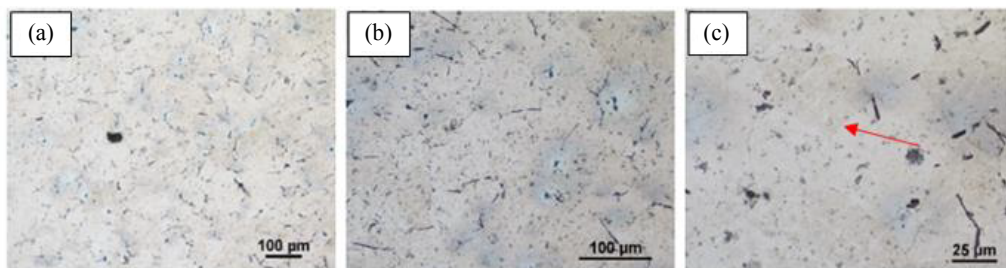


Figure 9: Optical micrographs of Alloy 1 in the z-direction after being solution heat treated at 510°C and aged at 160°C for 20h (a) 100x, (b) 200x (c) 500x.

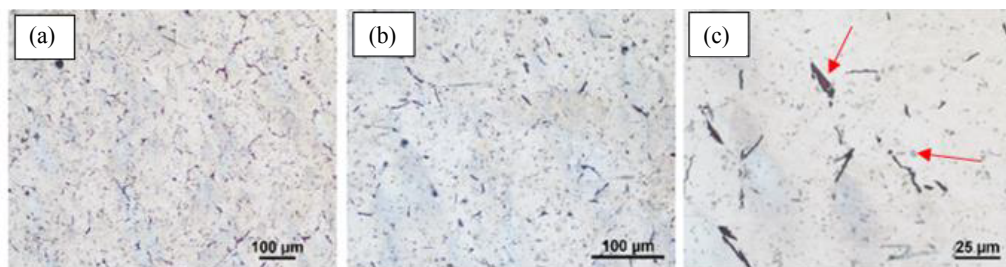


Figure 10: Optical micrographs of Alloy 1 in the x-direction after being solution heat treated at 510°C and aged at 160°C for 20h (a) 100x (b) 200x (c) 500x.

anticipated, the matrix exhibited a uniform distribution of alloying elements believed to represent the strengthening precipitates.

In order to confirm the presence of a fine strengthening network in the Al-Cu-Ag-Mg alloy, TEM was employed for Alloy 1 in the post-process solution heat treated and peak aged condition. Selective TEM images for this material is shown in Figures 13 and 14 for the [001] and near [111] zone axes, respectively. The strengthening precipitate θ' ,

which forms as thin plates on the {100} planes of the aluminum matrix, are readily visible in Figure 13. Two variants of θ' are exhibited as plate edges on the {100} planes. The θ' precipitates are evenly dispersed throughout the matrix and having plate diameters of approximately 30 to 50 nm. Figure 14, which was obtained at the near [111] zone axis, shows three variants of Ω precipitates on edge, which are believed to be the three possible variants of the $(001)_{\Omega} \parallel (111)_{\alpha}$ orientation relationship when observed for this zone axis. This has been confirmed

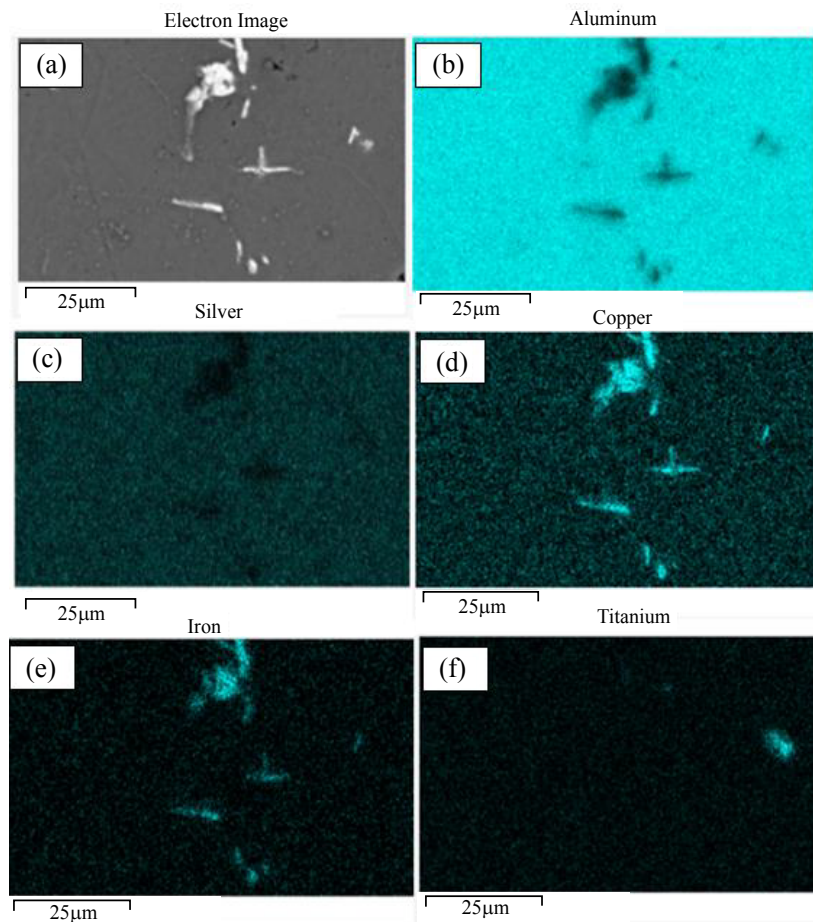


Figure 11: (a) SEM images of mapping area; (b) EDS map of aluminium; (c) EDS map of silver; (d) EDS map of copper; (e) EDS map of iron; (f) EDS map of titanium.

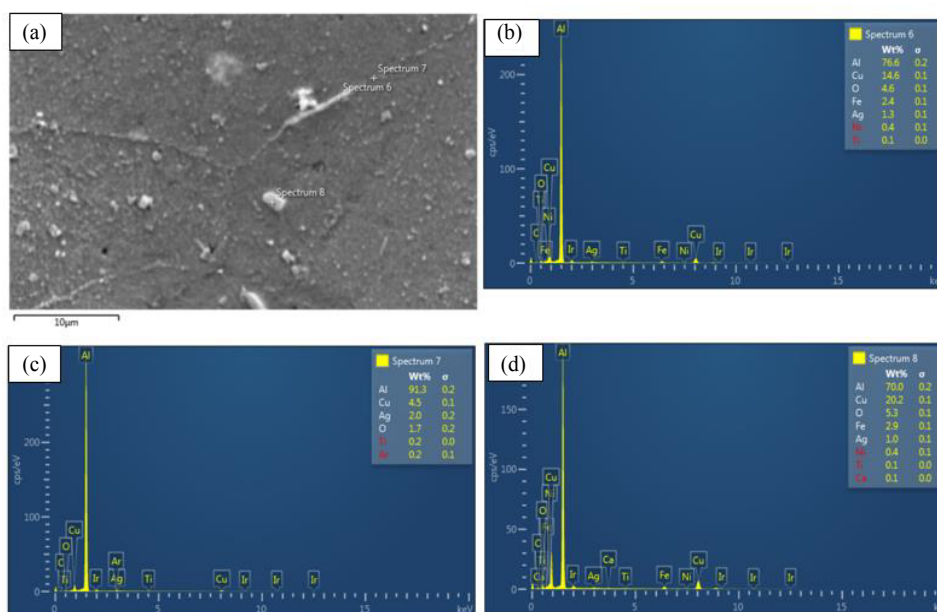


Figure 12: (a) Electron image indicating locations of point EDS measurements; (b) EDS Spectrum 6, long thin white constituent; (c) EDS Spectrum 7, grain boundary; (d) EDS Spectrum 8, round constituent.

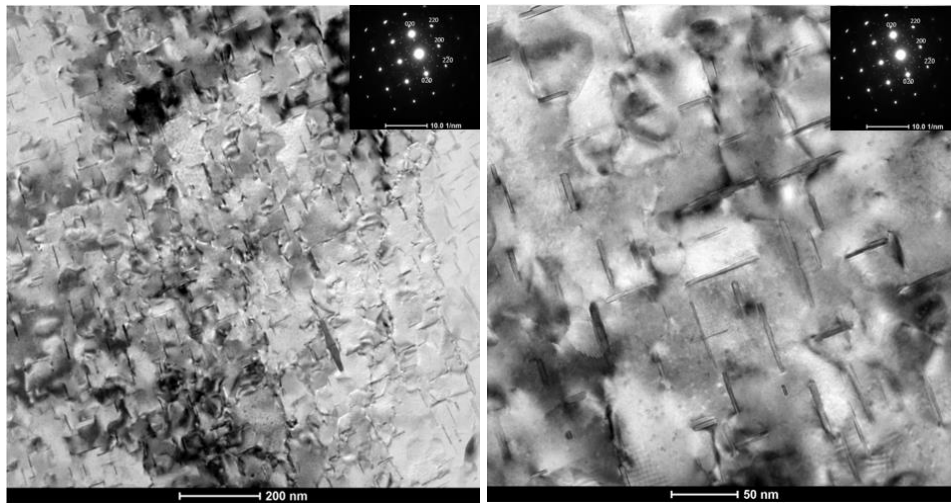


Figure 13: TEM images showing θ' precipitates in Alloy 1 in the peak-aged condition, with the diffraction pattern obtained for the [001] zone axis.

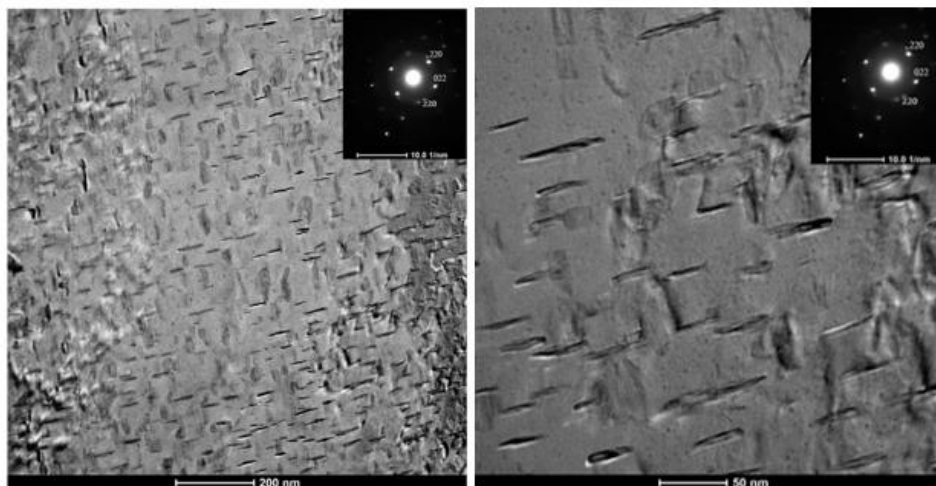


Figure 14: TEM images showing Ω precipitates in Alloy 1 in the peak-aged condition, with the diffraction pattern obtained for the near [111] zone axis.

by prior research, which showed at least three variants of Ω observable along the $\langle 111 \rangle_{\alpha}$ direction [14,22,38]. The Ω also exhibited a uniformly distributed network and was similar in size to θ' . Based on this analysis, and confirmed through microhardness measurements, the θ' and Ω formed within this system is capable of demonstrating highly effective precipitation strengthening.

Conclusion

Experiments were conducted on several alloys representing the Al-Cu-Ag-Mg system to determine the applicability of using these alloys for AM. Alloys were formulated and prepared utilizing a powder blending technique using a pre-alloyed master alloy powder containing Al, Mg, Ti, and Zr with elemental powders of pure Cu and Ag. These powders were processed using laser-based directed energy deposition to produce specimens that were treated to represent the post-process aged only and post-process solution heat treated and aged conditions. Optical microscopy of all alloys showed the presence of limited spherical porosity but no indication of solidification cracking occurring during the builds. Microhardness and microstructural characterization was

then conducted. Results of this investigation showed that an aluminum alloy containing between 6 and 8% Cu and 1 to 4% Ag, while also containing 0.3% Mg, Ti, and Zr, displayed excellent response to precipitation strengthening when solutionized at 510°C and aged at durations between 16 and 20 hours. Many of the alloys evaluated also displayed appreciable strengthening when subjected to post-process aging only at 160°C. Alloys that were completely solutionized and aged after processing were able to achieve microhardness values exceeding 180 VHN, which are significantly higher than the commonly used Al-10Si-0.5Mg alloy for AM processes. The high microhardness achieved with the experimental alloy could be attributed to a uniformly distributed network of fine θ' and Ω precipitates, which was confirmed through TEM. Depending upon the desired post processing treatment (aging only or solutionizing and aging), the results indicate that an alloy composition within this system may be defined to provide optimal strength.

References

1. Hatch JE (1984) Aluminum: Properties and Physical Metallurgy. United States.

2. Davis J (1998) Metals Handbook Desk Edition. ASM International.
3. Material Data Sheet (2014) EOS Aluminum AlSi10Mg. EOS GmbH.
4. Pennsylvania State University (2018) U.S. Provisional Patent Application 62/642,076.
5. Ding Y, Muñiz-Lerma JA, Trask M, Chou S, Walker A, et al. (2016) Microstructure and mechanical property considerations in additive manufacturing of aluminum alloys. *MRS Bulletin* 41: 745-751.
6. <https://www.imetllc.com/training-article/mechanisms-strengthening-aluminum/>
7. Cross C, Olsen D, Liu S (2003) Handbook of Aluminum: Welding Aluminum (2003), Marcel Dekker, Inc. (utilizing data from W. Pumphrey and D. Moore, Cracking during and after solidification in some aluminum-copper-magnesium alloys, *J Inst Metals*, 1948).
8. Taminger K, Hafley RA (2002) Characterization of 2219 Aluminum Produced by Electron Beam Freeform Fabrication. 13th Solid Freeform Fabrication Symposium, Austin, TX; United States.
9. Al-Obaisi AM, El-Danaf EA, Ragab AE, Soliman MS (2016) Precipitation Hardening and Statistical Modeling of the Aging Parameters and Alloy Compositions in Al-Cu-Mg-Ag Alloys. *J Mater Eng Perform* 25: 2432-2444.
10. Cross CE (2005) Hot Cracking Phenomena in Welds. Springer-Verlag Berlin Heidelberg.
11. Devinent SM, Devletian JH, Gedeon SA (1988) Weld properties of the newly developed 2519-T87 aluminum armor alloy. *Weld J* 67: 33-43.
12. Macchi C, Somoza A, Ferragut R, Dupasquier A, Polmear IJ (2009) Aging Processes in Al-Cu-Mg Alloys with Different Cu/Mg Ratios. *Phys Status Solidi* 6: 2322-2325.
13. Gable BM, Zhu AW, Shiflet GJ, Starke Jr EA (2008) Assessment of the aluminum-rich corner of the Al-Cu-Mg-(Ag) phase diagram. *CALPHAD: Comput. Coupling Phase Diagrams Thermochem* 32: 256-267.
14. Gazizov M, Kaibyshev R (2017) Precipitation structure and strengthening mechanisms in an Al-Cu-Mg-Ag alloy. *Mater Sci Eng A* 702: 29-40.
15. Vietz JT, Polmear IJ (1966) The influence of small additions of silver on the aging of aluminum alloys: observations on Al-Cu-Mg alloys. *J Inst Met* 94: 410-419.
16. Polmear IJ (1964) The effects of small additions of silver on the aging of some aluminum alloys. *Transactions of the Metallurgical Society of AIME* 230.
17. Teleshov VV, Kaputkin EY, Golovleva, Kosmacheva NP (2005) Temperature Ranges of Phase Transformations and Mechanical Properties of Alloys of the Al-Cu-Mg-Ag System with Various Cu/Mg Ratios. *Met Sci Heat Treat* 47: 18-23.
18. Chester RJ, Polmear IJ (1980) TEM Investigations of Precipitation in Al-Cu-Mg-Ag and Al-Cu-Mg Alloys. *Micron* 11: 311-312.
19. Castillo LD, Lavernia EJ (2000) Microstructure and Mechanical Behavior of Spray-Deposited Al-Cu-Mg-(Ag-Mn) Alloys. *Metall Mater Trans A* 31: 2287-2289.
20. Li Y, Liu Z, Xia Q, Bai S, Chen X (2011) Effects of Aging Temperature on the Precipitation Behavior of Ω Phase in an Al-Cu-Mg-Ag Alloy. *Met Mater Int* 17: 1-6.
21. Xiao DH, Wang JN, Ding DY, Chen SP (2002) Effect of Cu Content on the Mechanical Properties of an Al-Cu-Mg-Ag Alloy. *J Alloys Compd* 343: 77-81.
22. Muddle BC, Polmear IJ (1989) The Precipitate Ω Phase in Al-Cu-Mg-Ag Alloys. *Acta Metallurgica* 37: 777-789.
23. Liu XY, Wang ZP, Fu BG, Long L, Zhang XL, et al. (2016) Effects of Mg content on the mechanical properties and corrosion resistance of Al-Cu-Mg-Ag alloy. *J Alloys Compd* 685: 209-215.
24. Hono K, Sakurai T, Polmear IJ (1995) Pre-Precipitate Clustering in Aged Aluminum Alloys. *Mater Sci Forum* 189: 249-254.
25. Ringer SP, Sakurai T, Polmear IJ (1996) Origins of Hardening in Aged Al-Cu-Mg-(Ag) Alloys. *Acta Materialia* 45: 3731-3744.
26. Reich L, Murayama M, Hono K (1998) Evolution of Ω phase in an Al-Cu-Mg-Ag alloy – a three-dimensional atom probe study. *Acta Materialia* 46: 6053-6062.
27. Bai S, Zhou X, Liu Z, Xia P, Liu M, et al. (2014) Effects of Ag variations on the microstructures and mechanical properties of Al-Cu-Mg alloys at elevated temperatures. *Mater Sci Eng A* 611: 69-76.
28. Hutchinson CR, Ringer SP (2000) Precipitation Processes in Al-Cu-Mg Alloys Microalloyed with Si. *Metall Mater Trans A* 3: 2721-2733.
29. Davis JR (1993) Aluminum and Aluminum Alloys. Materials Park, OH: ASM International.
30. DeGeuser F, Bley F, Deschamps A (2010) Early stages of Ω phase precipitation in Al-Cu-Mg-Ag observed in situ with and without applied stress by small angle x-ray scattering. *Proceedings of the 12th International Conference on Aluminum Alloys*, Yokohama, Japan, pp: 475-480.
31. Huang BP, Zheng ZQ (1998) Independent and Combined Roles of Trace Mg and Ag Additions in Properties Precipitation Process and Precipitation Kinetics of Al-Cu-Li-(Mg)-(Ag)-Zr-Ti Alloy. *Acta Materialia* 46: 4381-4393.
32. Olefjord I, Karlsson A (1986) Aluminium Technology. The Institute of Metals, London, 383.
33. Snow Z, Martukanitz R, Joshi S (2018) Additive Manufacturing (submitted for publication).
34. Martukanitz RP, Michnuk PR (1982) Sources of porosity in gas metal arc welding of aluminium alloys. *Aluminium*, pp: 276-279.
35. <http://resources.renishaw.com/en/download/data-sheet-alsi10mg-0403-400-w-powder-for-additive-manufacturing--73122>
36. <http://www.matweb.com/search/datasheettext.aspx?matguid=20817c80e16042dd8672bf001bd7863e>
37. Davis JR (1993) ASM Specialty Handbook: Aluminum and Aluminum Alloys. ASM International.
38. Lewandowski JJ, Seifi M (2016) Metal additive manufacturing: A review of mechanical properties. *Annu Rev Mater Res* 46: 151-186.